

PRESSURE LIMIT OF HYDROGEN SPONTANEOUS IGNITION IN A T-SHAPED CHANNEL

Bragin, M.V., Makarov, D.V., and Molkov, V.V.*

Hydrogen Safety Engineering and Research Centre (HySAFER), University of Ulster, Newtownabbey, BT37 0QB, Northern Ireland, UK

Abstract

This paper describes a large eddy simulation model of hydrogen spontaneous ignition in a T-shaped channel filled with air following an inertial flat burst disk rupture. This is the first time when 3D simulations of the phenomenon are performed and reproduced experimental results by Golub et al. (2010). The eddy dissipation concept with a full hydrogen oxidation in air scheme is applied as a sub-grid scale combustion model to enable use of a comparatively coarse grid to undertake 3D simulations. The renormalization group theory is used for sub-grid scale turbulence modelling. Simulation results are compared against test data on hydrogen release into a T-shaped channel at pressure 1.2-2.9 MPa and helped to explain experimental observations. Transitional phenomena of hydrogen ignition and self-extinction at the lower pressure limit are simulated for a range of storage pressure. It is shown that there is no ignition at storage pressure of 1.35 MPa. Sudden release at pressure 1.65 MPa and 2.43 MPa has a localised spot ignition of a hydrogen-air mixture that quickly self-extinguishes. There is an ignition and development of combustion in a flammable mixture cocoon outside the T-shaped channel only at the highest simulated pressure of 2.9 MPa. Both simulated phenomena i.e. the initiation of chemical reactions followed by the extinction, and the progressive development of combustion in the T-shape channel and outside, have provided an insight into interpretation of the experimental data. The model can be used as a tool for hydrogen safety engineering in particular for development of innovative pressure relief devices with controlled ignition.

Keywords

Hydrogen, spontaneous ignition, large-eddy simulation, pressure relief device, eddy dissipation concept, detailed chemistry

Nomenclature

a	Speed of sound, m/s	V	Volume, m ³
A_r	Pre-exponential factor	$x_{i,j,k}$	Spatial coordinates, m
CFL	Courant-Friedrichs-Lewy number	Y	Mass fraction
C	Hydrogen concentration in a mixture, % by volume	<i>Greek</i>	
$C_{j,r}$	Molar concentration of species j in reaction r	β_r	Temperature exponent for r -th reaction
C_{RNG}	RNG LES constant, $C_{RNG} = 0.157$	Δ_{CV}	Control volume characteristic size, m
c_p	Specific heat capacity of mixture at constant pressure,	Δt	Time step, s
$c_p = \sum_m c_{p_m} Y_m$		γ	Specific heat ratio
D	Diffusion coefficient, m ² /s	$\gamma_{j,r}$	Third-body efficiency of the j -th species in the r -th reaction
E	Total energy, J/kg, $E = h - p/\rho + u^2/2$	μ	Dynamic viscosity, Pa·s
E_r	Activation energy for the reaction, J/kmol	μ_s	Parameter of RNG LES model, Pa·s,
g	Gravitational acceleration, m/s ²	$\mu_s = \bar{\rho}(0.157V_{CV}^{1/3})^2 \sqrt{2\tilde{S}_{ij}\tilde{S}_{ij}}$	
$H(x)$	Heaviside function	$u'_{i,r}$	Stoichiometric coefficient for reactant i in reaction r
H_c	Heat of combustion, J/kg	$u''_{i,r}$	Stoichiometric coefficient for product i in reaction r
h	Enthalpy, J/kg, $h = \int_{298.15}^T c_p dT$	$\eta'_{j,r}$	Rate exponent for reactant species j in reaction r
k	Thermal conductivity, W/m/K	$\eta''_{j,r}$	Rate exponent for product species j in reaction r
$k_{f,r}$	Forward rate constant for reaction r , consistent units	ρ	Density, kg/m ³ , $\rho = (pM)/(RT)$
$k_{b,r}$	Backward rate constant for reaction r , consistent units	τ	Timescale, s
L	Length scale, m	τ_η	Kolmogorov timescale, s
L_{SGS}	Sub-grid length scale, m, $L_{SGS} = C_{LES}V^{1/3}$	Γ	Net effect of third bodies on the reaction rate
M	Molecular mass, kg/kmole, $M = \sum_m V_m M_m$	<i>Subscripts and superscripts</i>	
N	Number of chemical species in the system; denotes Pr or Sc numbers in RNG equation	a	Air
Pr	Prandtl number, $Pr = \mu c_p / k$,	E	Source term in energy conservation equation
p	Pressure, Pa	eff	Effective value
$R_{i,r}$	Arrhenius molar rate of creation/destruction of specie i in reaction r , consistent units	H_2	Hydrogen
R	Universal gas constant, 8314.4 J/K/kmol	i,j,k	Spatial coordinate indexes
\tilde{S}_{ij}	Rate of strain tensor, s ⁻¹	m	m -th component of gas mixture
Sc	Schmidt number, $Sc = \mu/\rho D$	n	Summation index over all species
T	Temperature, K	SGS	Sub-grid scale
		r	Reaction index
		t	Turbulent
		<i>Stoich</i>	Stoichiometric
		0	Initial conditions

* Corresponding author. Tel: +44 289 036 8731; Fax: +44 289 036 8726; E-mail address: v.molkov@ulster.ac.uk

t	Time, s	Bars	
$u_{i,j,k}$	Velocity components, m/s	$\bar{\quad}$	LES filtered quantity
u'	Root-mean square of sub-grid scale velocity component, m/s	\sim	LES mass-weighted filtered quantity
U	Velocity scale, m/s	$*$	Fine scale quantities

1. Introduction

Safety is the main “non-technical” barrier for the emerging hydrogen economy. It is well-known that a sudden hydrogen release from a high pressure equipment into air can be spontaneously ignited at pressures far below of storage pressures up to 100 MPa used in today’s hydrogen and fuel cell applications [1, 2]. The phenomenon was firstly observed in experiments by Wolanski and Wojcicki [3] and was named as “diffusion” mechanism of spontaneous ignition. In spite of recent experimental and numerical studies there is still a lack of understanding and validated models able to reproduce the pressure limit of spontaneous ignition of hydrogen, especially in complex geometries like pressure relief devices (PRD) requiring 3D simulations. As a result, little practical recommendations exist to control conditions of spontaneous ignition and its transition to sustained jet fire.

Numerical studies by Bazhenova et al. [4], Liu et al. [5], and Xu et al. [6, 7] were focused on unconfined release from high-pressure storage directly into the atmosphere. While spontaneous ignition for direct release into the atmosphere was predicted by numerical simulations, no experimental proof exists up to date. However, spontaneous ignition was observed in experiments that included pipes located downstream of a rupture disk. Such experiments were performed by different groups including Dryer et al. [8], Mogi et al. [9], Golub et al. [10], Pinto et al. [11], etc.

Dryer et al. [8] reported that spontaneous ignition events are statistically distributed in a narrow pressure range of 2.04-2.21 MPa, with zero probability for membrane failure pressures less than 2.04 MPa and certain inflammation for failure pressures above 2.21 MPa at their experimental set up. In addition to identifying a minimum pressure below which no spontaneous ignition can be observed, it is found that reducing the length of the 1.27 cm (1/2”) NPT pipe nipple to 3.81 cm (1.5”) led to no spontaneous ignition at all failure pressures even up to 5.66 MPa. Authors [8] speculate on the importance of the initial stage of a membrane rupture on the mixing and subsequent spontaneous ignition process. They concluded that at low pressures, the chemical ignition time becomes the limiting factor, while at high pressures the mixing time to achieve significant flammable mixture volume limits the process.

Recent experimental study by Golub et al. [1, 2] argues on spontaneous ignition in a T-shaped channel for initial hydrogen pressure in the range 1.2-2.9 MPa. However, there is some ambiguity in published results of this study with statements of spontaneous ignition at 2.9 MPa in one paper and 2.43 MPa in another.

Numerical studies by Wen et al. [7, 12] confirmed the significance of a membrane opening time on the spontaneous ignition process. The 2D analysis of pressure-boundary rupture rate on hydrogen spontaneous ignition during release through a 3 mm hole in a wall of 0.1 mm thickness directly to atmosphere was carried out in [7]. Characteristic cell sizes used were 15-30 μm across the contact surface. This simulation corresponds to a scenario of unconfined release for which no experimental evidence exists. It was found that if the rupture rate is below a certain threshold value, there would be no spontaneous ignition. As the rupture rate increases, the temperature of the shock heated region grows more quickly owing to earlier flow expansion and once the rupture rate is sufficiently high, spontaneous ignition can occur. Hydrogen releases through a length of a tube 30-60 mm long and 3-6 mm internal diameter for storage pressures in a range 5-15 MPa were simulated in [12]. It was demonstrated that spontaneous ignition is governed by focusing of reflected from the tube wall shocks.

Lee and Jeung [13] investigated the effect of a burst disk shape on the ignition process at pressure of a burst disk rupture of 8.6 MPa and release into a tube. Cartesian grid with a cell size of 19 μm was used. The burst disk had a semi-spherical shape. However, an instant opening of the disk was applied in simulations. The spontaneous ignition first occurred in a boundary layer and consequently spread throughout a cross-section of the tube, i.e. through the contact surface between air and hydrogen where mixing takes place, similar to our previous 3D study with an instant opening of a flat membrane [14].

Simulations of hydrogen spontaneous ignition in air using the model accounting for viscous gas transport, multi-component diffusion, heat transfer, and incorporating a kinetic scheme of hydrogen oxidation with 9 equations were performed by Golub et al. [10]. The authors studied experimentally and numerically in 2D axisymmetric formulation the self-ignition in cylindrical and rectangular tubes and concluded that governing mechanism for hydrogen spontaneous ignition is diffusion ignition on the contact surface assisted by the boundary layer effects. Combustion starts as kinetic one and then acquires diffusion character. Heat release and flame turbulence intensify mixing of reagents and such burning cloud may propagate along the tube far enough. Simulation with and without the boundary layer were also carried out and a conclusion is drawn that when boundary layer is not taken into account, ignition occurs at the tube axis, whereas it occurs near the wall if boundary layer is taken into account.

2D numerical simulations of the phenomenon were carried out by Pinto et al. [11]. Axisymmetric Euler equations and detailed chemical reactions mechanism were employed to simulate the behaviour of the hydrogen jet discharged from a storage vessel at pressures 10-70 MPa and temperature 300 K at an early stage of the leakage. The reduced kinetic mechanism by Petersen and Hanson [15] with 9 species (H_2 , O_2 , O , H , OH , HO_2 , H_2O_2 , H_2O , and N_2) and 18 elementary reactions was applied. Chemical reactions were treated by a point implicit way to avoid stiffness. Uniform grid with a cell size of 20x20 μm was used to carry out simulations. Dependencies of the length, where the self-ignition occurs on the pressure in high-pressure chamber were obtained experimentally not only for smooth, but also for screwed tubes. It was found that screwed tubes produce some difficulty for spontaneous ignition affecting the boundary layer. Numerical simulations were reported only for one case of 10 mm diameter tube with 50 mm length and 3.8 MPa initial hydrogen pressure, but no comparison to experimental data has been made.

In study by Yamada et al. [16] the model [11] had been improved by adding viscosity effects. The governing equations used were the compressible 2D axisymmetric Navier-Stokes equations, the conservation of mass, total energy, chemical species, and the equation of state. The same reduced kinetic mechanism was applied [15]. The governing equations were discretized in a finite difference formulation. The convective terms are evaluated using the second-order explicit Harten-Yee non-MUSCL modified-flux type TVD scheme, considering the properties of the hyperbolic equations. The viscous terms are evaluated with the standard second-

order central difference formulae. The time integration method is the second-order Strang-type fractional step method. Grid with cell size of 20-45 μm was used to carry out simulations. Three inlet pressures were studied – 3.6, 5.3 and 21.1 MPa, estimated from choked conditions at the exit resulting from initial pressure in the large hydrogen tank of 6.8, 10 and 40 MPa. The tube had a 4.8 mm diameter and a length of 71 mm. It was found that a high-temperature area appears near the exit of the tube. The vortex generated near the edge of the exit was observed similarly to experimental results [9] and our numerical simulations [7]. The vortex plays an important role in mixing the hydrogen provided from the tube with surrounding air. It was shown that for a pressure of 3.6 MPa the spontaneous ignition does not occur in the vortex region; for a pressure of 5.3 MPa the shock wave retains a high temperature for spontaneous ignition, but chemical reactions do not continue long around the exit of the tube; and only for the pressure of 21.1 MPa combusting area remains. The authors also compared release from the tube and hole for the same tube diameter. It was shown that in the case of release from the hole, the confinement prevents the development of vortices and mixing of hydrogen with surrounding air in the recirculation zone.

To the best knowledge of authors of this paper, all simulations of hydrogen spontaneous ignition by the “diffusion” mechanism so far were carried out in 2D formulations, including axisymmetric, due to an understandable wish of researchers to have as fine mesh as possible to directly resolve the phenomenon. The large eddy simulation (LES) model developed and described in this paper employs a coarser 3D grid. This increase in mesh size is “compensated” by an advanced sub-grid scale (SGS) modelling of the combustion by the eddy dissipation concept with a detailed chemistry and the turbulence by the renormalization group (RNG) theory. The aim of this study is a model development and reproduction of experimental results obtained in a complex realistic geometries, where 2D simulations cannot be applied. This work aims to gain insights into transitional phenomena on the lower pressure limit of spontaneous ignition and assess the model’s predictive capability against experimental data obtained in a 3D geometry of the T-shaped channel at different pressures [1, 2], which is a mock-up of PRD.

2. The LES model

The LES technique is widely applied to solve scientific and engineering problems, including in the area of hydrogen safety. The LES model used in this study has been previously applied to simulate dynamics of spontaneous ignition of hydrogen emerging into air within simple geometries [14]. In this paper the model is described for the first time in full detail. The FLUENT software is used as the computational engine.

2.1. Conservation equations

The governing equations, employed for LES, are filtered over the control volume three-dimensional instantaneous conservation equations for mass, momentum (Navier-Stokes), energy, and species for compressible Newtonian fluid

$$\frac{\partial \bar{\rho}}{\partial t} + \frac{\partial}{\partial x_j} (\bar{\rho} \tilde{u}_j) = 0, \quad (1)$$

$$\frac{\partial \bar{\rho} \tilde{u}_i}{\partial t} + \frac{\partial}{\partial x_j} (\bar{\rho} \tilde{u}_i \tilde{u}_j) = -\frac{\partial \bar{p}}{\partial x_i} + \frac{\partial}{\partial x_j} \left(\mu_{eff} \left(\frac{\partial \tilde{u}_i}{\partial x_j} + \frac{\partial \tilde{u}_j}{\partial x_i} - \frac{2}{3} \frac{\partial \tilde{u}_k}{\partial x_k} \delta_{ij} \right) \right) + \bar{\rho} g_i, \quad (2)$$

$$\begin{aligned} & \frac{\partial}{\partial t} (\bar{\rho} \tilde{E}) + \frac{\partial}{\partial x_j} (\tilde{u}_j (\bar{\rho} \tilde{E} + \bar{p})) = \\ & = \frac{\partial}{\partial x_j} \left(\frac{\mu_{eff} c_p}{Pr_{eff}} \frac{\partial \tilde{T}}{\partial x_j} - \sum_m \tilde{h}_m \left(-\frac{\mu_{eff}}{Sc_{eff}} \frac{\partial \tilde{Y}_m}{\partial x_j} \right) + \tilde{u}_i \mu_{eff} \left(\frac{\partial \tilde{u}_i}{\partial x_j} + \frac{\partial \tilde{u}_j}{\partial x_i} - \frac{2}{3} \frac{\partial \tilde{u}_k}{\partial x_k} \delta_{ij} \right) \right) + \sum_m R_m H_C, \quad (3) \end{aligned}$$

$$\frac{\partial}{\partial t} (\bar{\rho} \tilde{Y}_m) + \frac{\partial}{\partial x_j} (\bar{\rho} \tilde{u}_j \tilde{Y}_m) = \frac{\partial}{\partial x_j} \left(\frac{\mu_{eff}}{Sc_{eff}} \frac{\partial \tilde{Y}_m}{\partial x_j} \right) + R_m. \quad (4)$$

The effective viscosity μ_{eff} is calculated using the renormalization group (RNG) theory [17]. The RNG model is capable to reproduce not only turbulent, but also transitional and laminar flows. At low Reynolds numbers the effective viscosity becomes equal to molecular viscosity. This allows the model to perform better in the vicinity of walls [18]. The effective viscosity is calculated in RNG model as

$$\mu_{eff} = \mu \left[1 + H \left(\mu_s^2 \mu_{eff} / \mu^3 - 100 \right) \right]^{1/3}, \quad (5)$$

where $\mu_s = \bar{\rho} (C_{RNG} V_{CV}^{1/3})^2 \sqrt{2 \tilde{S}_{ij} \tilde{S}_{ij}}$, $H(x)$ is Heaviside function.

In highly turbulent regions of the flow $\mu_{eff} \approx \mu_s$ and the RNG model reduces to the Smagorinsky model. In laminar flow regions the argument of Heaviside function becomes negative and the model recovers molecular viscosity, $\mu_{eff} = \mu$. The effective Prandtl and Schmidt numbers are calculated following the RNG theory by purely theoretical equations [17]

$$\left| \frac{1/N_{eff} - 1.3929}{1/N - 1.3929} \right|^{0.6321} \left| \frac{1/N_{eff} + 2.3929}{1/N + 2.3929} \right|^{0.3679} = \frac{\mu}{\mu_{eff}}, \quad (6)$$

where N stands for laminar Prandtl or Schmidt numbers. Laminar Prandtl and Schmidt numbers are calculated according to kinetic theory.

2.2. Combustion model

The Eddy Dissipation Concept (EDC) model [19] with updates that incorporates detailed Arrhenius chemical kinetics in turbulent flames was applied as the combustion sub-model. EDC gives an expression for a combustion rate based on an assumption that chemical reactions occur in so-called fine structures of Kolmogorov's scale where the dissipation of turbulence energy takes place. In a flow of moderate to intense turbulence these fine structures are concentrated in isolated areas occupying only a small fraction of the flow. The characteristic size of the fine structures is much smaller than a LES filter width (cell size in our case), and it needs to be computed as a function of flow parameters and a cell size.

In the EDC model adopted in FLUENT a source term in the species transport equation (4) is modelled as

$$R_m = \frac{\rho(\xi^*)^2}{\tau^* [1 - (\xi^*)^3]} (Y_m^* - Y_m), \quad (7)$$

where R_m is a net rate of production of specie m by chemical reactions, ξ^* is the length fraction of the fine scale turbulent structures where the reaction occurs, Y_m^* is the fine scale species mass fraction (specie m) after reacting over the time τ^* , Y_m is a species mass fraction for specie m in the surrounding fine scales state. The multiplier in (7) with a square of the length fraction of fine scales represents the mass exchange between the surrounding and fine structure regions. The length fraction of fine structures is evaluated in this LES model similar to EDC RANS model as

$$\xi^* = C_\xi u_\eta / u_{SGS}, \quad (8)$$

where the volume fraction constant is taken as $C_\xi = 2.1377$ similar to RANS. The upper limit $\xi^* = 1$ is applied when the fine scales velocity is larger than residual SGS velocity.

The scale of a LES residual velocity at the sub-grid scale (SGS) level is

$$u_{SGS} = \mu_t / (\rho \cdot L_{SGS}), \quad (9)$$

where μ_t is turbulent viscosity, and the SGS length scale is determined as

$$L_{SGS} = C_{RNG} V^{1/3}. \quad (10)$$

The Kolmogorov's velocity u_η is

$$u_\eta = \left(\frac{\mu \cdot u_{SGS}^3}{\rho \cdot L_{SGS}} \right)^{1/4}, \quad (11)$$

where μ is laminar viscosity.

Characteristic sub-grid eddy and Kolmogorov's timescales are respectively

$$\tau_{SGS} = L_{SGS} / u_{SGS}, \text{ and} \quad (12)$$

$$\tau_\eta = \left(\frac{\mu \cdot L_{SGS}}{\rho \cdot u_{SGS}^3} \right)^{1/2}. \quad (13)$$

The volume fraction of the fine scales is calculated as ξ^{*3} and species are assumed to react in the fine structures over a time scale

$$\tau^* = C_\tau \tau_\eta, \quad (14)$$

where a time scale constant is taken equal to $C_\tau = 0.4082$ similar to applied in the EDC RANS model.

Magnussen [20] assumes that all the fine scales in the cell are perfectly stirred reactors with a residence time τ^* . Combustion at the fine scales is assumed in this model to take place as a constant-pressure reactor. The reactor type is determined by the choice of a mixing rate $1/\tau^*$ and a time-step Δt . In FLUENT initial conditions at the constant pressure reactor are taken as the current species and temperature in the cell. Arrhenius reactions governed by equation (15) proceed over the time scale τ^* . The *in situ* adaptive tabulation ISAT algorithm [21], offering substantial reductions in run-times by up to three orders of magnitude, is applied.

All of the reactions considered in the chemical mechanism involved are elementary (reversible). For reversible reaction the molar rate of creation or destruction of species i in reaction r is given by equation (15)

$$\hat{R}_{m,R} = \Gamma \left(\nu_{m,r}'' - \nu_{m,r}' \right) \left(k_{f,r} \prod_{n=1}^N [C_{n,r}]^{\nu_{n,r}'} - k_{b,r} \prod_{n=1}^N [C_{n,r}]^{\nu_{n,r}''} \right), \quad (15)$$

where N is number of chemical species in the system; $\nu_{m,r}'$ is stoichiometric coefficient for reactant m in reaction r ; $\nu_{m,r}''$ is stoichiometric coefficient for product m in reaction r ; $k_{f,r}$ is forward rate constant for reaction r ; $k_{b,r}$ is backward rate constant for reaction r . Γ represents the net effect of third bodies on the reaction rate and is given by

$$\Gamma = \sum_{n=1}^N \gamma_{n,r} C_n, \quad (16)$$

where $\gamma_{m,r}$ is the third-body efficiency of m -th species in the r -th reaction.

The forward rate constant for reaction r without pressure dependency is computed in conventional form of Arrhenius equation

$$k_{f,r} = AT^{\beta_r} \exp(-E_r/RT). \quad (17)$$

All reactions are reversible, the backward rate constant for reaction r is calculated from the forward rate (17) and the equilibrium constant K_r using the equation

$$k_{b,r} = k_{f,r} / K_r. \quad (18)$$

The equilibrium constant K_r computed as

$$K_r = \exp\left(\frac{\Delta S_r^0}{R} - \frac{\Delta H_r^0}{RT}\right) \cdot \left(\frac{P_{atm}}{RT}\right)^{\sum_{i=1}^N (v_{m,r}'' - v_{m,r}')} , \quad (19)$$

where P_{atm} denotes atmospheric pressure (101,325 kPa). The term within the exponential function represents the change in Gibbs free energy and its components are computed as

$$\frac{\Delta S_r^0}{R} = \sum_{i=1}^N (v_{m,r}'' - v_{m,r}') \frac{S_m^0}{R}, \quad (20)$$

$$\frac{\Delta H_r^0}{RT} = \sum_{i=1}^N (v_{m,r}'' - v_{m,r}') \frac{h_m^0}{RT}, \quad (21)$$

where S_m^0 and h_m^0 are entropy and enthalpy respectively of the m -th species respectively evaluated at temperature T and atmospheric pressure.

Specific heats of mixtures were approximated as piecewise-polynomial functions of temperature with polynomial coefficients calculated according to mass-weighted mixing law.

2.3. Chemical reaction mechanism

In this study the detailed 21-step chemical reaction mechanism of hydrogen combustion in air employing 37 elementary reactions is applied [22]. The effect of nitrogen chemistry is taken into account by considering detailed mechanism of NO formation. The specific reaction rate constants are given in Table 1. The forward reaction rate constants are presented in the table, and backward rates for reversible reactions are calculated through the equilibrium constants (18).

Table 1. Specific reaction rate constants [22].

No.	Reactions	A , KJ/mol	β_r	E_r , mol/m ³
1	H+O2=OH+O	2.00E+14	0.00	70.30
2	H2+O=OH+H	1.80E+10	1.00	36.93
3	H2O+O=OH+OH	5.90E+09	1.30	71.25
4	H2+OH=H2O+H	1.17E+09	1.30	15.17
5	H+O2+M=HO2+M	2.30E+18	-0.8	0.00
	Third-body chaperon efficiencies H2/1./ H2O/6.5/ O2/0.4/ N2/0.4/			
6	H+HO2=OH+OH	1.50E+14	0.00	4.20
7	H+HO2=H2+O2	2.50E+13	0.00	2.93
8	OH+HO2=H2O+O2	2.00E+13	0.00	4.18
9	H+H+M=H2+M	1.80E+18	-1.00	0.00
	Third-body chaperon efficiencies H2/1./ H2O/6.5/ O2/0.4/ N2/0.4/			
10	H+OH+M=H2O+M	2.20E+22	-2.00	0.00
	Third-body chaperon efficiencies H2/1./ H2O/6.5/ O2/0.4/ N2/0.4/			
11	HO2+HO2=H2O2+O2	2.00E+12	0.00	0.00
12	H2O2+M=OH+OH+M	1.30E+17	0.00	190.38
13	H2O2+OH=H2O+HO2	1.E+13	0.00	7.53
14	O+HO2=OH+O2	2.E+13	0.00	0.00
15	H+HO2=O+H2O	5.E+12	0.00	5.90
16	H+O+M=OH+M	6.2E+16	-0.60	0.00
	Third-body chaperon efficiencies H2O:5, others 1			
17	O+O+M=O2+M	6.17E+15	-0.50	0.00
18	H2O2+H=H2O+OH	1.E+13	0.00	15.02
19	H2O2+H=HO2+H2	4.79E+13	0.00	33.26
20	O+OH+M=HO2+M	1.E+16	0.00	0.00
21	H2+O2=OH+OH	1.7E+13	0.00	200.0
	Nitrogen Chemistry			
22	O+N2=N+NO	1.82E+14	0.00	319.02
23	O+NO=N+O2	3.8E+09	1.00	173.11
24	H+NO=N+OH	2.63E+14	0.00	210.94

25	$\text{NO}+\text{M}=\text{N}+\text{O}+\text{M}$	3.98E+20	-1.50	627.65
26	$\text{N}_2+\text{M}=\text{N}+\text{N}+\text{M}$	3.72E+21	-1.60	941.19
27	$\text{N}_2\text{O}+\text{O}=\text{NO}+\text{NO}$	6.92E+13	0.00	111.41
28	$\text{N}_2\text{O}+\text{O}=\text{N}_2+\text{O}_2$	1.E+14	0.00	117.23
29	$\text{N}_2\text{O}+\text{N}=\text{N}_2+\text{NO}$	1.E+13	0.00	83.14
30	$\text{N}+\text{HO}_2=\text{NO}+\text{OH}$	1.E+13	0.00	8.31
31	$\text{N}_2\text{O}+\text{H}=\text{N}_2+\text{OH}$	7.6E+13	0.00	63.19
32	$\text{HNO}+\text{O}=\text{NO}+\text{OH}$	5.01E+11	0.50	8.31
33	$\text{HNO}+\text{OH}=\text{NO}+\text{H}_2\text{O}$	1.26E+12	0.50	8.31
34	$\text{NO}+\text{HO}_2=\text{HNO}+\text{O}_2$	2.E+11	0.00	8.31
35	$\text{HNO}+\text{HO}_2=\text{NO}+\text{H}_2\text{O}_2$	3.16E+11	0.50	8.31
36	$\text{HNO}+\text{H}=\text{NO}+\text{H}_2$	1.26E+13	0.00	16.63
37	$\text{HNO}+\text{M}=\text{H}+\text{NO}+\text{M}$	1.78E+16	0.00	203.7

3. Experimental setup for the model validation

The geometry of a high pressure system and connected to it T-shaped channel, mimicking PRD, is taken from the experimental study of the spontaneous ignition [1]. The high pressure system consists of a 210 mm long tube with 16 mm internal diameter (ID) followed by a 280 mm long tube with 10 mm ID at the end of which a flat burst disk, made of copper or aluminium with cuts facilitating failure, is located followed by a mock-up PRD open to atmosphere (Fig.1). The PRD has a 48 mm long axial channel of 6.5 mm ID with a flat end, and two radial channels on opposite sides of the axial channel to vent hydrogen to atmosphere. Each radial channel has 6.25 mm length and 4 mm ID (distance from the end connected to the atmosphere of one radial channel to the end of another is 19 mm). Radial channels are flushed with the axial channel end wall and positioned so that the edge of each side channel touches tangentially the flat end wall of the axial channel. The burst disk opening was estimated in [1] as about ten microseconds thus creating conditions for better mixing of hydrogen with air during the opening as compared to non-realistic instant opening. To register spontaneous ignition a light sensor was installed along the axis of radial channels of the PRD. Temperature behind the shock wave reflected from the flat end wall was estimated as more than twice higher than the temperature behind the incident shock wave. Golub et al. [1] stated that when the initial pressure in high pressure chamber did not exceed 1.2 MPa the light sensor did not record any signal, and when pressure was 2.9 MPa the ignition was registered [1]. Unfortunately, there is no information published on storage pressures in between these two values. However, it is stated later in [2] that light was registered at pressure 2.43 MPa.

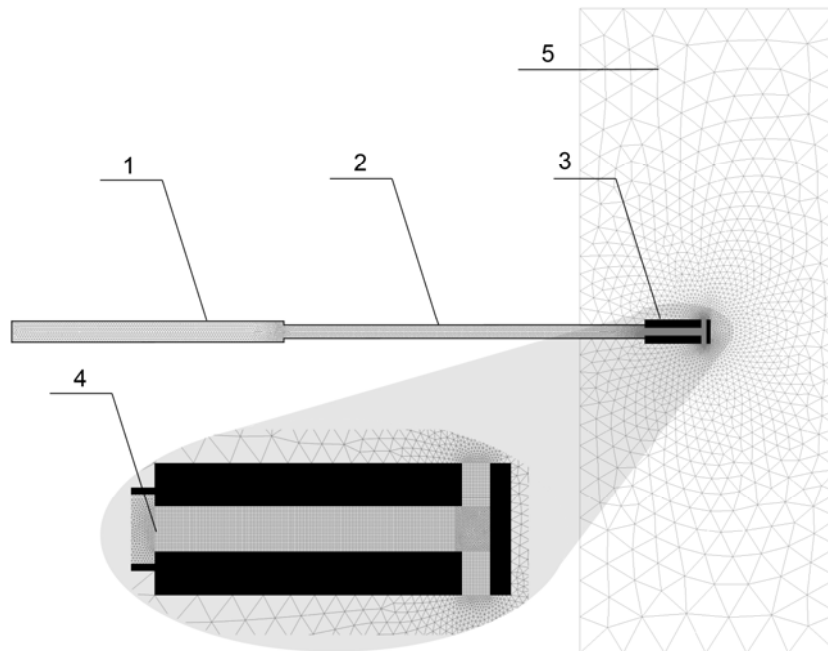


Figure 1. The geometry and computational domain: 1 and 2 – high pressure tubes, 3 – PRD, 4 – burst disk, 5 – external domain.

3.1. Numerical details

The 3D grid was created using GAMBIT tool of the CFD package FLUENT 6.3.26, which realises control-volume based finite-difference method. The axial and radial channels of the PRD were meshed with a hexahedral grid with a uniform control volume (CV) size of about 400 μm both along the axial channel and in its cross-section, excluding the intersection zone. The intersection area of the axial and the radial channels was meshed with tetrahedral CVs with size of about 200 μm , i.e. the largest CV size used in numerical simulations of the spontaneous ignition phenomenon up to date. This is due to the application of the LES technique requiring 3D domain and thus larger CV size to simulate a problem in reasonable computation time. The high-pressure chamber was meshed by tetrahedrons with the smallest CV size of about 250 μm clustered near the membrane of the PRD and rapidly increasing away from it reaching the maximum cell width of 10 mm at the far end. The total number of control volumes in the computational domain was equal to a moderate number of 417,685 cells.

Non-slip impermeable adiabatic boundary conditions were used on walls. Non-reflecting open “pressure-far-field” boundaries were used outside of the PRD. The high pressure system was modelled as closed to exclude potential effects of inlet boundary conditions on the process. This assumption is valid because the observation time in simulation is less than a time required for rarefaction wave to reach the far end of the high-pressure system. Four cases are presented in current paper to illustrate change in the process dynamics with initial hydrogen pressure in the high-pressure system $p_0 = 1.35, 1.65, 2.43$ and 2.90 MPa. Initial temperature $T_0 = 300$ K and the mole fraction of hydrogen equal to 1 were assumed in the high-pressure system before the burst disk rupture in all cases. Low pressure chamber was filled with air (0.23 mass fraction of oxygen and 0.77 of nitrogen) at $p_0 = 0.101$ MPa and $T_0 = 300$ K.

The solver used explicit linearisation of the governing equations with explicit method for solution of linear equation set. A second order upwind scheme with AUSM flux splitting was applied for flow discretisation. The four step Runge-Kutta algorithm was employed for advancement of simulations in time. The time step was determined from Courant-Friedrichs-Lewy condition, where the CFL number was equal to 0.2 to ensure stability.

3.2. Burst disk opening modelling

The burst disk opening is expected to play an important role in the process of ignition due to effect on mixing between hydrogen and air. A modelling strategy used in this work is presented below. Following Spence and Woods [23], the following formula is applied to calculate an opening time of a diaphragm

$$t = k(\rho b d / p)^{1/2}, \quad (22)$$

where ρ is the density of the diaphragm material, b and d are thickness and diameter of the diaphragm respectively, and the values of k are found to be in a range 0.91-0.93 [12]. Density of annealed copper is 8900 kg/m^3 . For example, for 2.9 MPa case, the opening time can be calculated as

$$t = 0.92(8900 \cdot 5 \cdot 10^{-5} \cdot 6.5 \cdot 10^{-3} / 2.9 \cdot 10^6)^{1/2} = 29.1 \text{ } \mu\text{s} \quad (23)$$

The opening of a membrane was approximated in simulations by 10 step-like process (see Fig. 2) with a time for each section given in Table 2 for four investigated cases.

Table 2. Opening times of sections for simulated cases.

Section	1	2	3	4	5	6	7	8	9	10
Opening time, μs [1.35 MPa case]	0	4.7	9.4	14.2	18.9	23.6	28.4	33.1	37.8	42.6
Opening time, μs [1.65 MPa case]	0	4.3	8.6	12.8	17.1	21.4	25.6	29.9	34.3	38.5
Opening time, μs [2.43 MPa case]	0	3.5	7.1	10.6	14.2	17.7	21.3	24.8	28.3	31.9
Opening time, μs [2.9 MPa case]	0	3.2	6.5	9.7	12.9	16.2	19.4	22.6	25.9	29.1

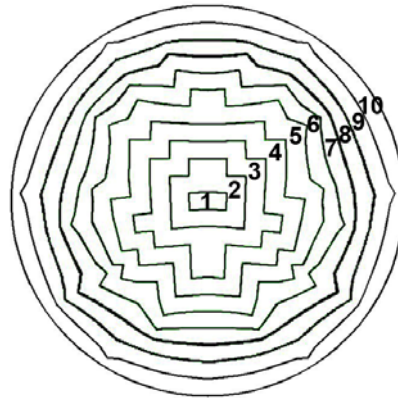


Figure 2. Step-like approximation of a burst disk rupture process: 1-10 are sections that open in series.

4. Results and discussion

4.1. Initial stage following the membrane rupture

Figure 3 shows dynamics of temperature and hydrogen mole fraction at an initial stage of hydrogen release into air in the mock up PRD with instant opening (left) and inertial opening (right) of the burst disk for initial pressure 1.35 MPa in the high pressure chamber. The inertial burst disk rupture process is accompanied by formation of an under-expanded jet from the changing open area of the membrane. A barrel-like structure can be seen for the case of inertial membrane opening (Fig.3, right). The opening of each next of 10 sections of the burst disk changes the barrel diameter to a larger one and the flow pattern looks similar to the multiple diamond-like pattern characteristic for this range of pressures. For the case of instant opening of an imaginary non-inertial membrane the shock heated zone in air is almost three times thicker compared to the inertial membrane rupture case at the same moment of time. The inertial opening of the membrane generates more intense mixing between hydrogen and air, including in the boundary layer of the axial channel walls. Maximum temperature in the shock-heated air is 50 K lower for the inertial membrane opening case. Thus, simulation of the burst disk opening is an important part for understanding of the phenomenon and predictive capability of the tool to be applied for hydrogen safety engineering.

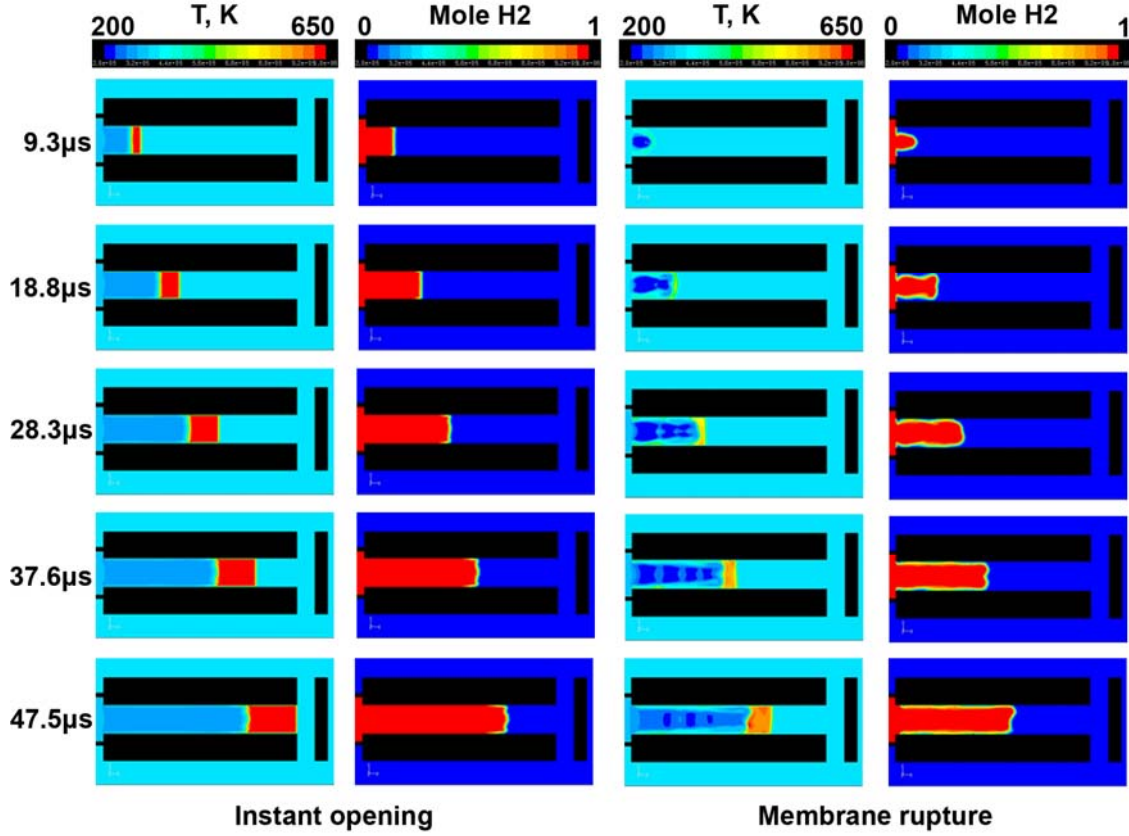


Figure 3. Dynamics of temperature and hydrogen mole fraction at the initial stage following a burst-disk rupture for instant opening (left) and inertial ten-step opening (right) for the 1.35 MPa case.

4.2. Reflection in a T-section

Analysis of gas dynamic equations shows that pressure wave reflections play a major role in triggering the spontaneous ignition process. One can estimate reflected pressure in a T-junction using 1D gas dynamic equations [24]. First, we estimate the Mach number M_S of the shock wave generated by the discontinuity (see Fig. 4a)

$$\frac{p_4}{p_1} = \left(1 + \frac{2\gamma_1}{\gamma_1 + 1}(M_S^2 - 1)\right) \left(1 - \frac{\gamma_4 - 1}{\gamma_1 + 1} \cdot \frac{a_1}{a_4} \cdot \frac{M_S^2 - 1}{M_S}\right)^{\frac{2\gamma_4}{\gamma_4 - 1}}, \quad (24)$$

where p_4/p_1 is initial hydrogen to atmospheric air pressure ratio when membrane is removed, γ_1 and γ_4 are specific heat ratio for air and pushing gas respectively (for our case $\gamma_1 = \gamma_4 = 1.4$), a_1/a_4 – ratio of air to hydrogen speed of sound.

Knowing M_S , we can calculate pressure p_2 behind the leading shock wave (propagating in air) [24]

$$p_2 = p_1 \left(\frac{2\gamma_1 M_S^2}{\gamma_1 + 1} - \frac{\gamma_1 - 1}{\gamma_1 + 1} \right). \quad (25)$$

And finally, calculate the pressure p_5 following normal reflection of leading shock wave (see Fig. 4b)

$$\frac{p_5}{p_2} = \frac{(3\gamma_1 - 1)p_2 / p_1 - (\gamma_1 - 1)}{(\gamma_1 - 1)p_2 / p_1 + (\gamma_1 + 1)}. \quad (26)$$

Calculations using Eqs. (24)-(26) and results of numerical simulation for the reflected shock pressure ratio are summarized in Table 3. Results of LES simulations are close to the theoretical predictions yet are by 8-10% above the theory.

Table 3. Calculated parameters for normal shock wave reflection using Eqs. (24)-(26).

Initial hydrogen pressure, MPa	1.35	1.65	2.43	2.9
Mach number of leading shock wave Eq.(24)	2.47	2.64	2.98	3.15
Pressure behind leading shock wave Eq.(25), MPa	0.7	0.8	1.04	1.16
Calculated reflected pressure Eq.(26), MPa	2.96	3.61	5.15	6.0
Simulated reflected pressure (LES), MPa	3.25	3.9	5.56	6.6

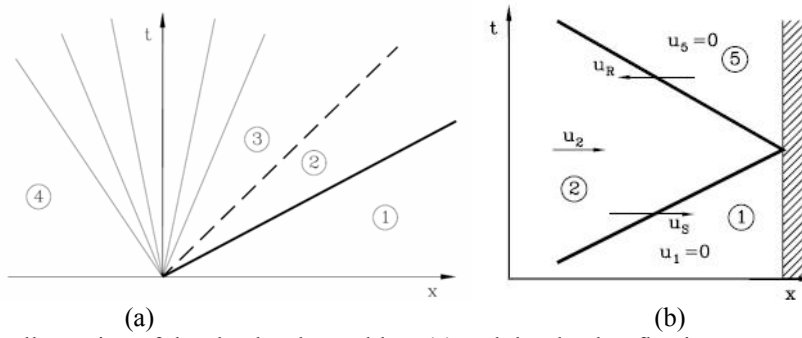


Figure 4. Illustration of the shock-tube problem (a) and the shock reflection process (b) [24].

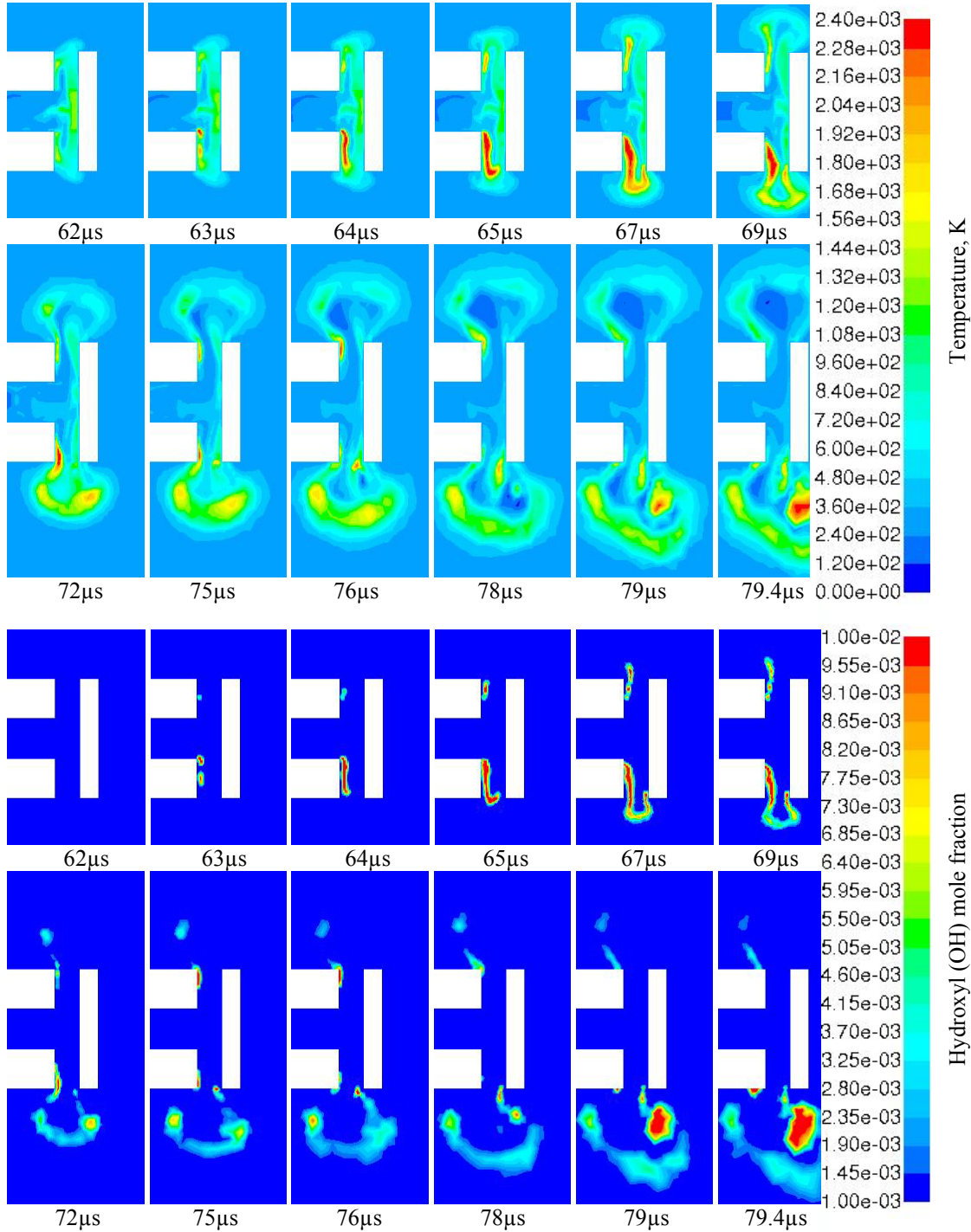


Figure 5. Temperature and hydroxyl mole fraction for 2.9 MPa case.

However, applicability of basic theories is often limited to simple scenarios, e.g. propagation of a normal shock wave through uniform mixture and reflection from a flat surface. If the mixture is not uniform or the shock is oblique and surface is not flat then simple methods are hardly applied. The case of T-shaped channel is even more complicated due to absence of hydrogen-air mixture in

an area of first reflection, i.e. the flat end wall of the axial channel, and presence of multiple reflections from curved surfaces of the channels.

Temperature and hydroxyl mole fraction profiles in the axial cross-section for cases with initial pressure in the high pressure chamber of 29 MPa and 24.3 MPa cases are presented in Figs. 5 and 6 respectively. It is clear that ignition is not possible immediately after the leading shock reflection since hydrogen has not been supplied to this area yet. Once the hydrogen flow diffracts around the edge from the axial into radial channels, it starts mixing with heated by shocks air. This provides the necessary conditions for ignition of the mixture. It can be seen that for both initial pressures combustion is initiated in the radial channel in a location which is closer to the upstream wall.

Larger high-temperature regions can be observed for 2.9 MPa case (Fig. 5) compared to 2.43 MPa case inside the PRD, but the difference is obvious when combusting mixture is pushed outside. At pressure 2.9 MPa a semi-spherical cocoon of a heated to critical conditions flammable hydrogen-air mixture is formed outside the PRD being followed by expanding hydrogen. Combustion is initiated in a number of spots within the cocoon (see snapshots of temperature and OH mole fraction at 79 μ s). The concentration of hydrogen in these spots outside the PRD just before the ignition is in the range 29-36% by volume. Thus, a conclusion can be drawn that the ignition by the “diffusion” mechanism takes place in the most reacting hydrogen-air mixtures. This external combustion is assumed to sustain a jet fire following the spontaneous ignition.

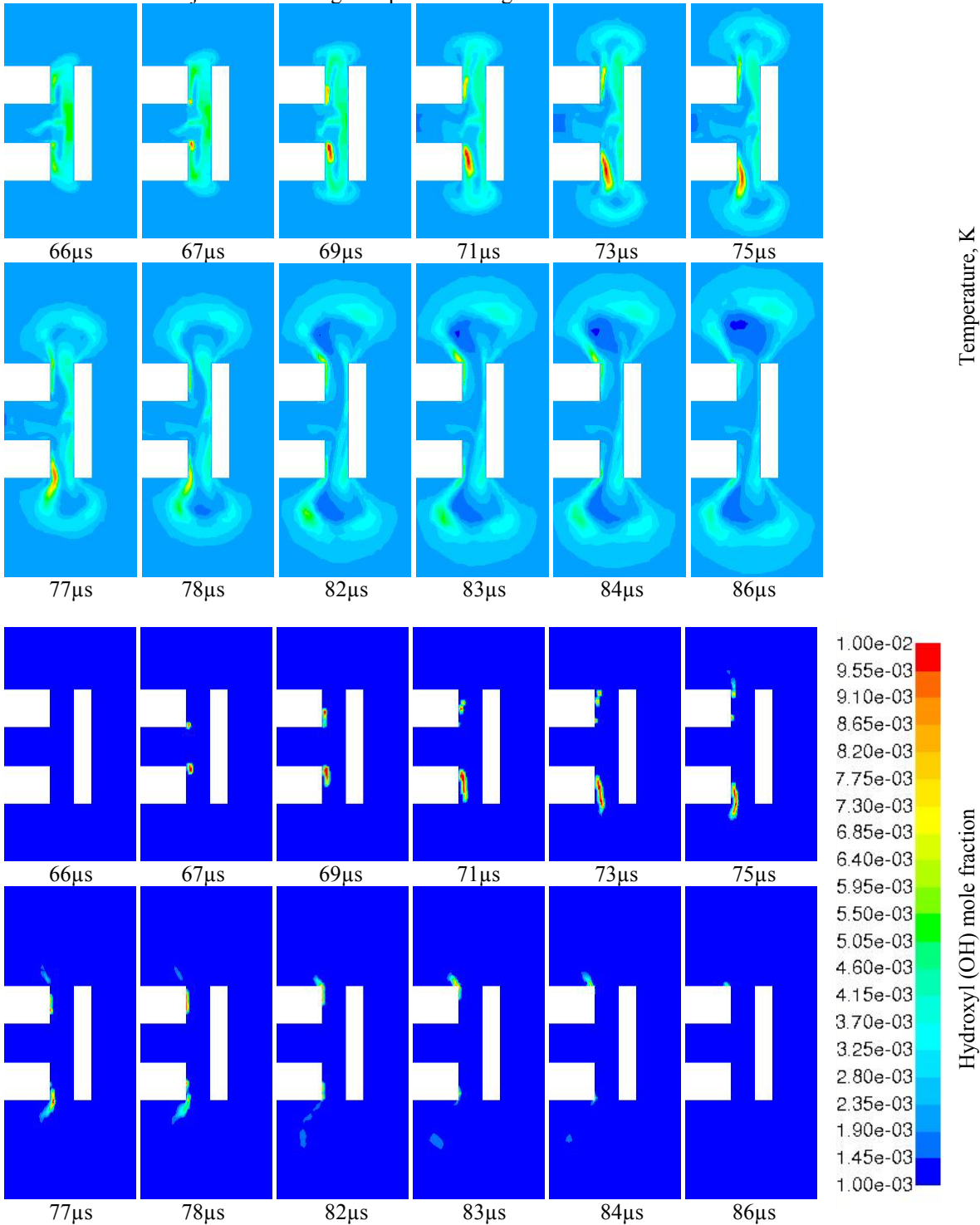


Figure 6. Temperature and hydroxyl mole fraction profiles for 2.4 MPa case.

In 2.43 MPa case (Fig. 6) the combustion is rather weak, compared to 2.9 MPa case, and the reacting mixture is dragged with the adjacent hydrogen flow, which leads to the elongation of combusting regions. Upon exit from the radial channels of the PRD, the flow undergoes an expansion and high-temperature regions disappear ceasing reaction and OH concentration, including the cooling role of pure hydrogen jet on the flammable mixture. The whole process from combustion initiation to self-extinction (disappearance of high temperature and OH mole fractions region) takes a little more than 10 μ s. This is sufficient to register the chemical reaction by a light sensor in the experiments.

It can be seen in Figs. 5 and 6 that the process is asymmetrical, i.e. the ignition in the upper radial channel is weaker than in the lower channel and for the case of 2.9 MPa it survives the expansion from only the lower channel, while the upper part is extinguished. This could be due to the asymmetrical opening of the membrane in simulations (see Fig. 2), which could reflect a stochastic character of the burst-disk rupture in the experiments. This result demonstrates a sensitivity of the spontaneous ignition phenomenon to the membrane rupture process that should be investigated further along with effect of other factors, e.g. air humidity, etc.

In the case of initial storage pressure 1.65 MPa an ignition spot is located not in the symmetry plane. Temperature and hydroxyl mole fraction dynamics are shown in Figs. 7 and 8 respectively in 3D. The combustion is located within the axial channel and propagated upstream of the flow rather than with the main flow. When oxygen in the boundary layer is consumed the chemical reaction is self-extinguished. Simulations explain why “ignition” was not reported in the experimental paper for this pressure. Indeed, the light sensor can register only the ignition in the radial channel and cannot see the process within the axial channel unless special arrangements are done, e.g. the axial channel has transparent walls.

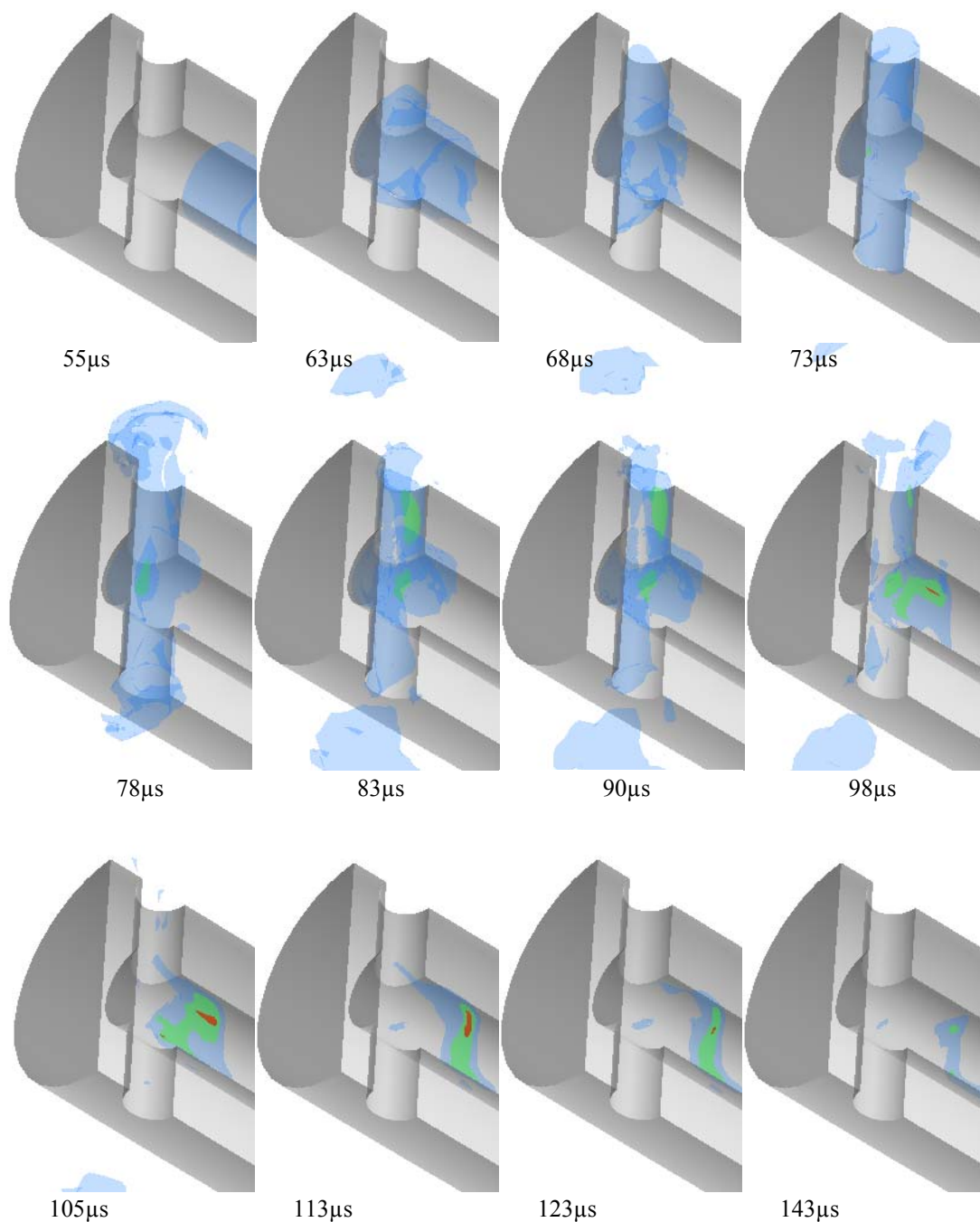


Figure 7. Temperature iso-surfaces during ignition for the initial hydrogen storage pressure 1.65 MPa. Blue – 550 K, Green – 1500 K, Red – 2400 K.

Figure 9 shows temperature dynamics for the 1.35 MPa case. Hydroxyl mole fraction dynamics is not presented, because OH concentration is of the order of 10^{-9} - 10^{-10} indicating that there is no combustion in the domain. Temperature scale in Fig. 9 is 0-1100 K. This is different from the scale 0-2400 K applied in previous Figures.

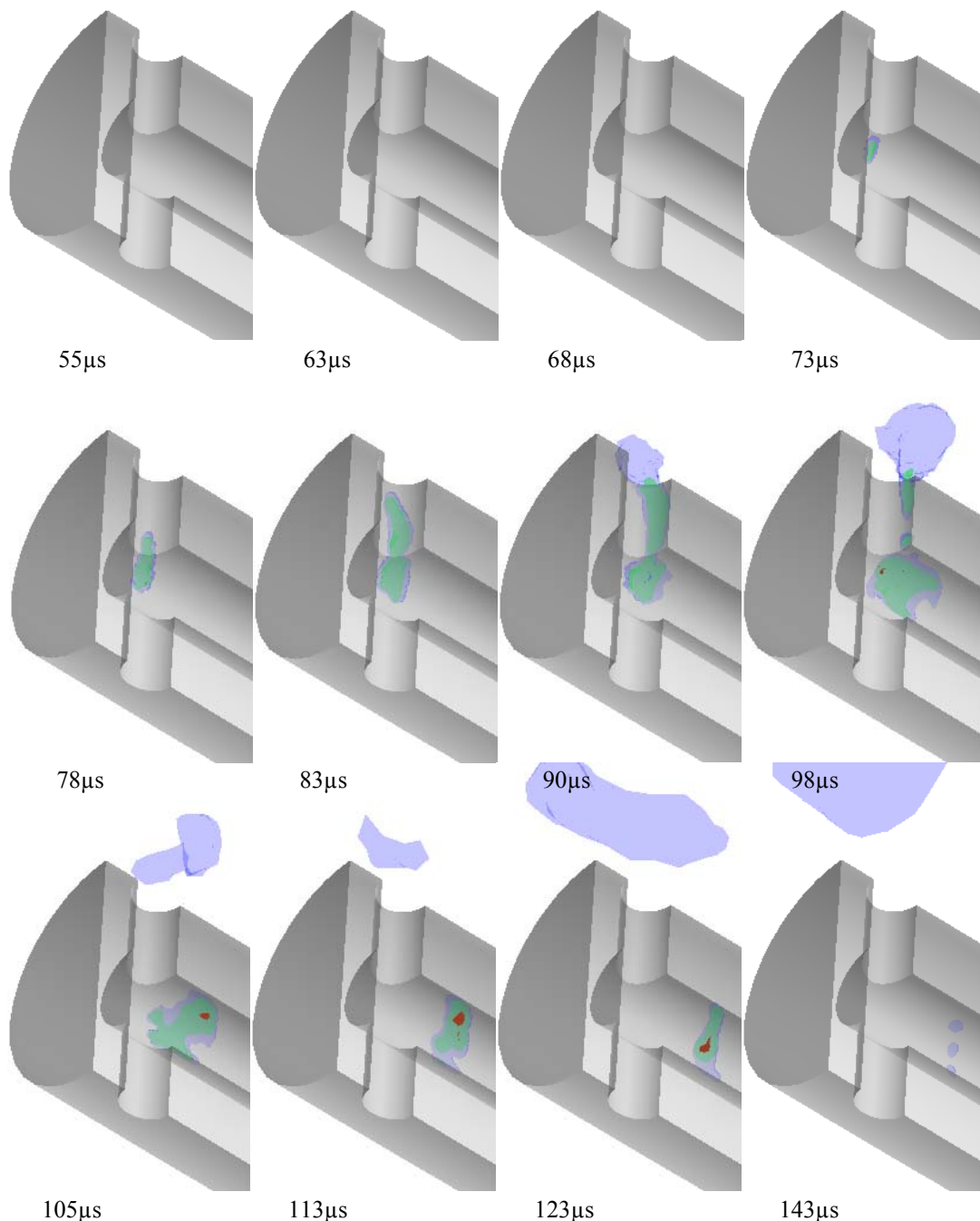


Figure 8. Hydroxyl mole fraction iso-surfaces during ignition for the initial hydrogen storage pressure 1.65 MPa. Blue – 0.0002, Green – 0.002, Red – 0.02.

Conclusions

The LES model based on the eddy dissipation concept with detailed Arrhenius kinetics for modelling of SGS combustion, and renormalization group theory for modelling of SGS turbulence is applied to gain an insight into the pressure limit of hydrogen spontaneous ignition during release into the T-shaped channel with air mimicking PRD. It is confirmed that a realistic inertial rupture of the flat burst disk indeed affects the mixing process between heated by shock air and cold expanding hydrogen as compared to the unreal instantaneous opening of the disk.

A series of numerical simulations of the process is performed at hydrogen storage pressures 1.35, 1.65, 2.43 and 2.9 MPa. Simulations have demonstrated that there is no ignition at pressure 1.35 MPa. There is an ignition followed by a self-extinction of reaction at storage pressures 1.65 and 2.43 MPa. The minimum pressure at which the ignition has been observed numerically is 1.65 MPa. However, the initial spot of combustion is quickly self-extinguished. The “sustainable” ignition has been achieved at pressure 2.9 MPa when multiple spots of combustion develop in the cocoon of the flammable mixture outside the PRD. The ignition by the “diffusion” mechanism is located in the most reacting hydrogen-air mixtures in the range of hydrogen concentrations 29-36% by volume. The pressure range 2.43-2.9 MPa can be considered as the pressure limit for spontaneous ignition of hydrogen in the studied

T-shaped geometry that could lead to the sustained jet flame. This study is in line with results of the experimental study [1, 2] yet explains a reported in the experiments “scattering” of the minimum ignition pressure in the range 2.43-2.9 MPa.

The important result of this work is development and validation of the LES EDC model that can be applied as a contemporary tool for hydrogen safety engineering, e.g. design of pressure relief devices.

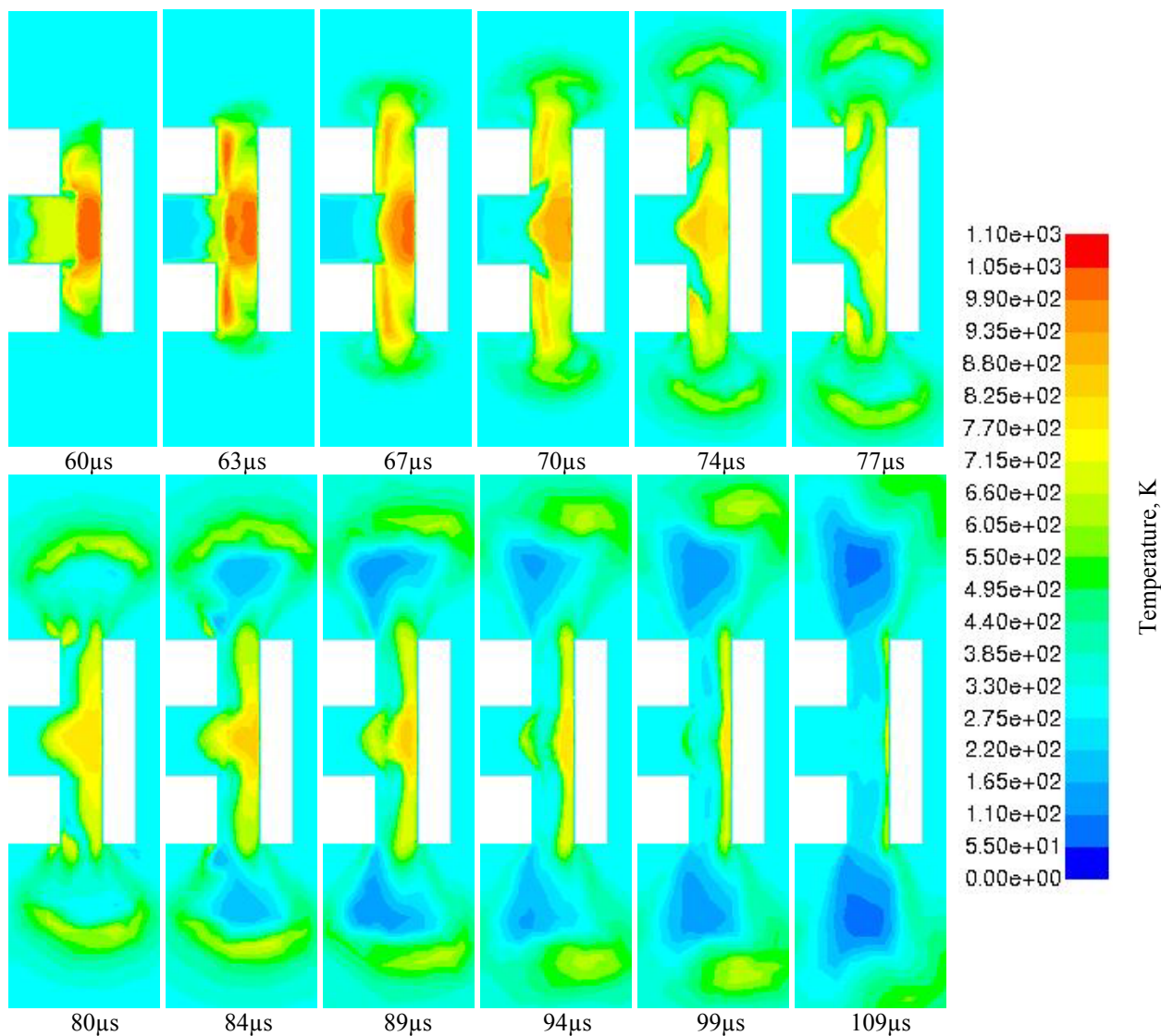


Figure 9. Temperature profiles across the symmetry plane for 1.35 MPa case.

References

1. Golub V.V., Volodin V.V., Baklanov D.I., Golovastov S.V., Lenkevich D.A., Experimental investigation of hydrogen ignition at the discharge into channel filled with air, In: *Physics of Extreme States of Matter*, ISBN 978-5-901675-96-0, Chernogolovka, 2010, pp.110-113.
2. Golub V.V., Private communication, 2010.
3. Wolanski, P. and Wojcicki, S., Investigation into the mechanism of the diffusion ignition of a combustible gas flowing into an oxidizing atmosphere, *Proceedings of the Combustion Institute*, **14**, 1972, pp. 1217-1223.
4. Bazhenova, T.V., Bragin, M.V., Golub, V.V. and Ivanov, M.F., Self-ignition of a fuel gas upon pulsed efflux into an oxidative medium, *Technical Physics Letters*, **32**, No. 3, 2006, pp. 269-271.
5. Liu, Y.-F., Tsuboi, N., Sato, H., Higashino, F., Hayashi, A.K. and Gakuin, A., Direct numerical simulation of hydrogen fuel jetting from high pressure tank, *Proceedings of the 20th International Colloquium on the Dynamics of Explosions and Reactive Systems*, 31 July - 5 August 2005, Montreal.
6. Xu, B.P., El Hima, L., Wen, J.X., Dembele, S., Tam, V.H.Y. and Donchev, T., Numerical study on the spontaneous ignition of pressurized hydrogen releases through a tube into air, *Journal of Loss Prevention in the Process Industries*, **21**, No. 2, 2008, pp. 205-213.
7. Xu, B.P., Wen, J.X., Dembele, S., Tam, V.H.Y. and Hawkworth, S.J., The effect of pressure boundary rupture rate on spontaneous ignition of pressurized hydrogen release, *Journal of Loss Prevention in the Process Industries*, **22**, No. 3, 2009, pp. 279-287.
8. Dryer, F.L., Chaos, M., Zhao, Z., Stein, J.N., Alpert, J.Y. and Homer, C.J., Spontaneous ignition of pressurized releases of hydrogen and natural gas into air, *Combustion Science and Technology*, **179**, No. 4, 2007, pp. 663-694.

9. Mogi, T., Kim, D., Shiina, H. and Horiguchi, S., Self-ignition and explosion during discharge of high-pressure hydrogen, *Journal of Loss Prevention in the Process Industries*, **21**, No. 2, 2008, pp. 199-204.
10. Golub, V.V., Baklanov, D.I., Golovastov, S.V., Ivanov, M.F., Laskin, I.N., Saveliev, A.S., Semin, N.V. and Volodin, V.V., Mechanisms of high-pressure hydrogen gas self-ignition in tubes, *Journal of Loss Prevention in the Process Industries*, **21**, No. 2, 2008, pp. 185-198.
11. Pinto, D., Aizawa, K., Liu, Y.F., Sato, H., Hayashi, A.K. and Tsuboi, N., Auto-ignition of high pressure hydrogen release. Proceedings of the 21st International Colloquium on the Dynamics of Explosions and Reactive Systems, 23-27 July 2007, Poitiers.
12. Wen, J.X., Xu, B.P., Tam, V.H.Y., Numerical study on spontaneous ignition of pressurized hydrogen release through a length of tube, *Combustion and Flame*, **156**, No. 11, 2009, pp. 2173-2189.
13. Lee, B.J. and Jeung, I.-S., Numerical study of spontaneous ignition of pressurized hydrogen release by the failure of a rupture disk into a tube. *International Journal of Hydrogen Energy*, **34**, 2009, pp.8763-8769.
14. Bragin, M. and Molkov, V., Physics of spontaneous ignition of high-pressure hydrogen release and transition to jet fire, Proceedings of the 3rd International Conference on Hydrogen Safety, 16-18 September 2009, Ajaccio, France. (Bragin, M.V., and Molkov, V.V., Physics of spontaneous ignition of high-pressure hydrogen release and transition to jet fire, *International Journal of Hydrogen Energy*, **36**, 2011, pp. 2589-2596).
15. Petersen, E.L., Davidson, D.F., Hanson, R.K. Ignition Delay Times of Ram Accelerator CH/O/Diluent Mixtures, *Journal of Propulsion and Power*, **15**:1, 1999, p. 82-91
16. Yamada, E., Watanabe, S., Hayashi, A.K., Tsuboi, N., Numerical analysis on autoignition of a high-pressure hydrogen jet spouting from a tube, *Proceedings of the Combustion Institute*, **32**, No. 2, 2009, pp. 2363-2369.
17. Yakhot, V. and Orszag, S., Renormalization group analysis of turbulence. I. Basic theory. *Journal of Scientific Computing*, **1**, 1986, pp.3-51.
18. Shah, R.K., Heikal, M.R., Thonon, B., and Tochnon, P. Progress in the numerical analysis of compact heat exchanger surfaces. In Hartnett, J. P. (Ed.) *Advances in Heat Transfer*, **34**, 2001, San Diego, USA, Academic Press.
19. Magnussen, B.F., On the structure of turbulence and a generalized eddy dissipation concept for chemical reactions in turbulent flow. Proceedings of the 19th American Institute for Aeronautics and Astronautics Aerospace Science Meeting, 12-15 January 1981, St. Louis.
20. Magnussen, B.F., Modelling of pollutant formation in gas turbine combustors based on the eddy dissipation concept. Proceedings of the CIMAC Conference, 4-9 June, 1989, Tianjin, China.
21. Pope, S.B., Computationally efficient implementation of combustion chemistry using in situ adaptive tabulation. *Combustion Theory and Modelling*, **1**, 1997, pp.41-63.
22. Gutheil, E., Balakrishnan, G. and Williams, F.A., Structure and extinction of hydrogen-air diffusion flames, In: Reduced kinetic mechanisms for applications in combustion systems (Peters, N. and Rogg, B. Eds.), Springer-Verlag, New York, 1993, p. 179.
23. Spence, D.A., and Woods, B.A., A review of theoretical treatments of shock-tube attenuation, *Journal of Fluid Mechanics*, **19**, 1964, pp. 161-174.
24. Sturtevant, B. and Liepmann, H.W. Lecture notes for the course in Nonsteady Gasdynamics. 2001. Available at <http://www.galcit.caltech.edu/%7Ejeshep/Ae237-2001/notes/guide.pdf>. Accessed October 2008.